J Supercond Nov Magn (2016) 29:1499–1507
DOI 10.1007/s10948-016-3449-7

ORIGINAL PAPER

Effect of Surface Roughness on the Magnetic Field Profile in the Meissner State of a Superconductor

Michael Lindstrom[1] · Alex C. Y. Fang[2] · Robert F. Kiefl[2,3]

Received: 4 November 2015 / Accepted: 2 February 2016 / Published online: 24 February 2016

Abstract It is well known that the London model (valid for a hard type II superconductor) predicts an externally applied magnetic field decays exponentially as a function of depth into the superconductor on a length scale λ. Direct measurements of the field profile using low energy μSR on high-Tc superconductors, such as $YBa_2Cu_3O_x$ measure deviations from a simple exponential decay. In particular, there is a short length scale δ close to the surface where the magnetic field does not decay. It has been proposed that this is due to surface roughness, which leads to a suppression of the order parameter near the surface. A model of surface roughness has been studied for the case of a sinusoidally modulated surface roughness on an isotropic superconductor showing that in some cases the profiles resulting from surface roughness may be qualitatively similar to the dead layer phenomena in that the field magnitude decay rate may be slowed near the surface relative to a flat interface but that for modest roughness, the quantitative value of the length over which the field decay is slowed is much smaller than the experiments measure. In this paper, we extend this work in two directions: firstly, by using atomic force microscopy data of $YBa_2Cu_3O_x$ crystals, we predict the expected field profiles within the context of the Isotropic London model of superconductivity given their actual surface geometry; and secondly, we consider how surface roughness could affect experimental values for λ and δ. The main finding is that roughness within an isotropic model does not produce the dead layers found in experiments on $YBa_2Cu_3O_x$. However, we suggest that roughness in a highly anisotropic superconductor could account for the observed dead layer.

Keywords Superconductor · Surface roughness · London equation

✉ Michael Lindstrom
mikel@math.ucla.edu

[1] Department of Mathematics, The University of California Los Angeles, Los Angeles, CA, USA

[2] Department of Physics and Astronomy, The University of British Columbia, Vancouver, BC, Canada

[3] TRIUMF, Vancouver, BC, Canada

1 Introduction

A superconductor is a metal or alloy that undergoes a phase transition at a critical temperature, below which its resistance drops to zero. One of the defining features of a superconductor which distinguishes it from a perfect conductor is the so called Meissner effect whereby an external applied magnetic field (below some critical field) is expelled as the superconductor is cooled below its critical temperature [1]. One of the early explanations for the Meissner state is based on the London equation, which predicts how the magnetic field $\mathbf{B}$ varies spatially inside a superconductor [1]. Employing Einstein summation notation, it states

$$B_i = \lambda^2 m_{k\ell} e_{\ell\sigma i} e_{k\tau j} \partial_{x_\sigma, x_\tau} B_j$$

for a length scale λ, a dimensionless mass tensor m, B_i being the ith component of $\mathbf{B}$, and the Levi-Civita symbol e [2]. In an isotropic superconductor, it simplifies to

$$\nabla \times \nabla \times \mathbf{B} = -\mathbf{B}/\lambda^2. \tag{1}$$

When (1) is coupled with the divergence-free condition of magnetic fields as given by Maxwell's equations

$$\nabla \cdot \mathbf{B} = 0, \tag{2}$$

it gives

$$\nabla^2 \mathbf{B} = \mathbf{B}/\lambda^2. \tag{3}$$

The length scale λ is called the London penetration depth. If a superconductor takes up the region in the $(x, y, z)-$coordinate space $z > 0$ and the applied magnetic field at the interface pointing in the $\hat{\mathbf{x}}$-direction is $B\hat{\mathbf{x}}$ for some $B > 0$ then the magnetic field within the superconductor is given by

$$\mathbf{B} = Be^{-z/\lambda}\hat{\mathbf{x}}.$$

Thus, as a function of depth z into a flat superconductor, the magnetic field magnitude decays exponentially with a length scale of λ. A more detailed theory of superconductivity uses the Ginzburg-Landau equations, which include a coherence length parameter ξ, which is the length scale over which the value of the order parameter changes. The London model is recovered for superconductors in which $\xi \ll \lambda$ [3], as is the case of the superconductor we study in this paper [4].

The London penetration depth is a fundamental quantity to measure in a superconductor because the magnitude of the order parameter given by the density of superconducting electrons n is directly related to λ with $\lambda = \sqrt{\frac{m_{\text{eff}}}{\mu_0 n q^2}}$. Here, m_{eff} is the effective mass of the moving charges, μ_0 is the permeability of free space, and q is the charge of each carrier. Understanding the superconductivity and the effects of doping relies heavily upon accurate measurements of λ.

There are notably two distinct types of superconductors. Above the critical field, a type I superconductor immediately allows for magnetic field penetration. In a type II superconductor, there are two critical fields H_{c1} and H_{c2}. Below H_{c1}, the external field is expelled as in a type I superconductor. Above H_{c1} but below H_{c2}, the material remains superconducting but the magnetic field penetrates in the form of a vortex lattice. It is only when the field exceeds H_{c2} that superconductivity is extinguished.

Depending on the field orientation, there are both in-plane ($a-$ and $b-$directions) and out-of-plane (c-direction) values of λ that can be measured. Normally, this anisotropy is described in terms of an effective mass tensor $1/\lambda^2 \propto n_s/m^*$ where m^* is the effective mass tensor and n_s is the scalar superfluid density. Experiments on $YBa_2Cu_3O_x$ find the in-plane λ's as $\lambda_a = 160$ nm and $\lambda_b = 103$ nm extrapolated to $T = 0$ [5]. Given another orientation, the through-plane value is $\lambda = \lambda_c \gg \lambda_{a,b}$ [6]. Absolute values of λ are difficult to measure reliably due to systematic errors associated with each experimental method and the fact the values depend sensitively on the the quality of crystals. Many early studies on polycrystals and thin films give very different results and longer penetration depths. The most common bulk methods are infrared absorption, microwave resonance, magnetic force microscopy (MFM), and tunnel diode resonator (TDR) [7, 8]. One also can use bulk muon spin rotation to measure the field distribution in the vortex state and extract the product of in plane penetration depths λ_a and λ_b [9]. The most direct method is to use low energy μSR to directly measure the field profile in the Meissner state [7]. There is generally reasonably good agreement between methods performed on highest quality single crystals [7].

$YBa_2Cu_3O_x$ is a type II superconductor with a planar crystal structure with highly anisotropic superconducting properties. It is a member of the copper oxide family of superconductors, where the main structural element is CuO_2 planes separated or spaced by other layers which may be used to control the carrier density or doping in the CuO_2 planes. The $YBa_2Cu_3O_x$ we study are made by the self-flux method using $BaZrO_3$ [10]. The crystals have a high level of purity, of the same quality of crystals where quantum fluctuations in resistivity have been measured [11]. They are mirror like in appearance and are approximately rectangular: 1 to 3 mm in the ab-plane and 0.1 to 0.3 mm in the c-direction [7].

Low energy μSR allows for a direct measurement of λ by measuring the profile of magnetic field penetration in $YBa_2Cu_3O_x$. These results have shown that near the interface, the magnetic field profile differs from a pure exponential decay predicted by the London equation with a flat interface [7]. There appears to be a short distance of size $\delta \approx 10$ nm over which the magnetic field magnitude does not change appreciably with depth, what we will refer to as a "dead layer." Understanding this phenomena is important because accurate measurements of λ rely upon models assuming a simple exponential decay [7] [12]. As the surfaces of the superconducting samples are known to be rough, a common speculation is that the non-exponential behavior near the interface is due to the surface roughness [7, 13]. Previous work modeling the effects of roughness with the superconductor surface given by $z = A\cos(\omega_x x)\cos(\omega_y y)$ has shown that roughness can alter the profile of the average field magnitude within a superconductor [14], where the averaging is done over x and y. Our work here will generalize the superconductor to have a surface given by $z = f(x, y)$ such that we can analyze experimentally measured surfaces instead of sinusoidal idealizations. See Fig. 1 for a sketch of the geometry. The sinusoidal modeling work showed that while roughness does not produce a perfect dead layer where there is no decay of the field, the roughness can yield a small depth over which the field decay is slowed. Such work suggested that for modest roughness amplitudes $A \sim \delta$ and spatial frequencies ω_x and ω_y with corresponding spatial wavelengths of size $\sim \lambda$, the roughness effects were not quantitatively consistent with experimental data. However, without knowing the value of A, the spatial frequencies present in the surface or localized behaviors of the magnetic field near surface anomalies, the work cannot provide conclusive evidence one way or the

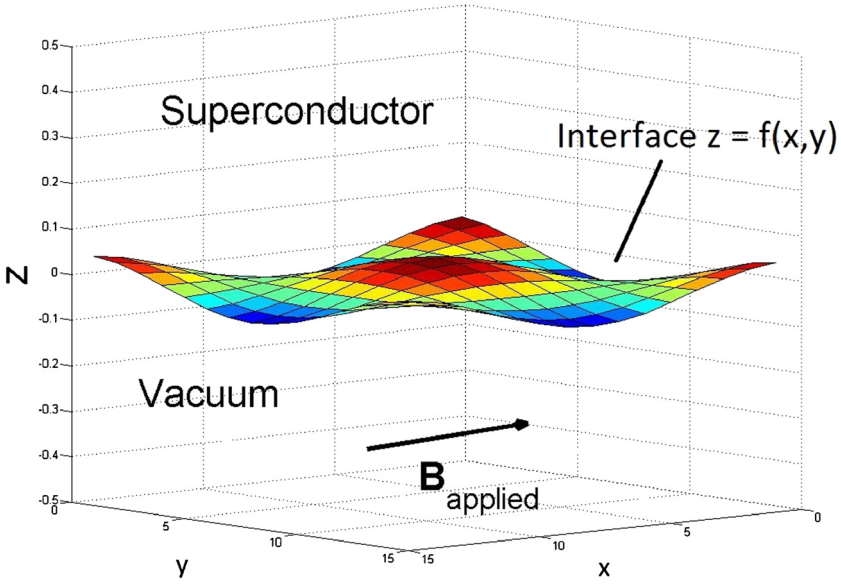

Fig. 1 This diagram illustrates the geometry that we model. The superconductor can be thought to take up the region in space $z \geq f(x, y)$, with the region $z < f(x, y)$ being a vacuum. A magnetic field $\mathbf{B}_{\text{applied}} = B\hat{\mathbf{x}}$ is applied far away from the superconductor, such that in the vacuum far from the interface ($z \to -\infty$), this applied field is recovered. Deep within the superconductor ($z \to \infty$), the London equation gives us that the field decays to zero

other for surface roughness being the cause of the altered decay rates.

In this paper, by using data collected through AFM measurements of $YBa_2Cu_3O_x$ crystals, we provide quantitative estimates of the values of λ and δ that could be obtained in the presence of roughness where we assume an isotropic value of $\lambda = \lambda_{\text{true}} = 110$ nm. The choice of adopting an isotropic model allows us to study the surface roughness in isolation from the anisotropy. The surface data we consider are given in Fig. 2.

One of the key results of this work is, in some senses, a non-result. In particular, we provide evidence that the slowed decay of the magnetic field strength near the superconductor-vacuum interface found in $YBa_2Cu_3O_x$ is likely not due to roughness in isolation and that we only expect a dead layer when there is roughness that is combined with the anisotropy of the material; indeed, by considering both local, rapidly changing surface features and large-scale surface features within the context of an isotropic superconductor, a region of non-negligibly slowed field decay is not found. We pose an explanation as to how an anisotropy could be combined with surface roughness to yield a slowed field decay rate (or in other words, a "dead layer" effect).

The paper is organized as follows: Section 2 provides a high-level overview of the numerical method we use to conduct our study and how it is validated; Section 3 outlines our key results for the effects of surface roughness; finally, we conclude our paper and discuss future work in Section 4.

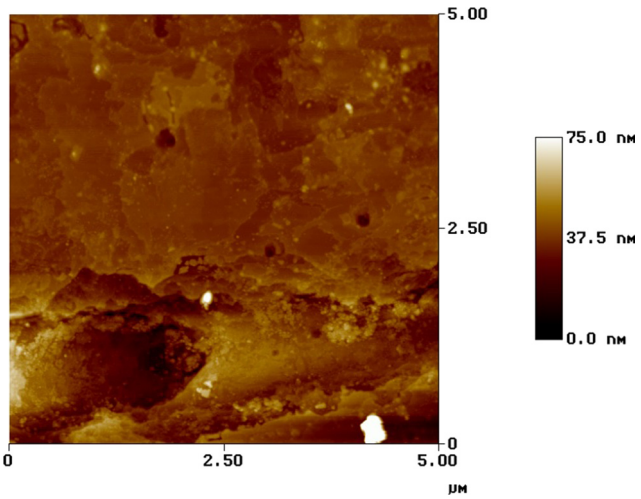

Fig. 2 Atomic Force Microscopy measurements of a $YBa_2Cu_3O_x$ surface as measured by [15]. We observe that the surface is not flat. There is a lot of roughness

2 Method of Study

The work here extends the numerical framework previously done in [14] to surfaces of arbitrary periodic shape. We refer the interested reader to this paper for a full discussion of the numerical formulation. This section explains briefly how the code has been extended and validated. A reader primarily interested in the results of this study can skip this section without any loss of continuity, although Section 2.3 may be recommended in understanding the discussion on the fitting parameters.

2.1 About the Numerical Framework

After nondimensionalizing and recasting the equations describing magnetic fields in free space and those describing magnetic fields in superconductors into an analytically equivalent form suitable for finite difference techniques,

a new coordinate system is introduced, one in which the rough interface given by $z = \epsilon \cos(\omega_x x)\cos(\omega_y y)$ becomes flat. Under such a transformation, the spatial derivatives in x, y, and z are rewritten in the new coordinate system which involves derivatives of $\epsilon \cos(\omega_x x)\cos(\omega_y y)$. In this case, the surface shape is given analytically and the $x-$ and y-derivatives could be computed as such. If the surface is only known experimentally at a discrete set of points $z_{ij} = z(x_i, y_j)$ where i and j are discrete indices on some finite range, the exact value of the derivatives may be unknown, but it is possible to compute the derivatives to an arbitrary order of accuracy with respect to spatial mesh size. To ensure agreement between the two codes (the code of [14] that we refer to as the analytic approach and this extension that we refer to as the discrete approach) to second-order accuracy, it is necessary to compute the derivatives of the surface to at least third-order accuracy. The entire framework for the analytic code was based on second-order finite differences and thus the discrete code is second-order accurate.

We also take a further precaution in dealing with the surface numerically in ensuring the surface is reasonably smooth. Because the London equation and the numerical formulations require two derivatives to be taken, having regions of discontinuity could pose problems to the numerics. The numerical method works for surfaces that are periodic in x and y. To deal with this in the case of the subsets we analyze in Section 3.3, we take each subset and produce a periodic surface through reflections, essentially repeating the surface four times in different orientations as in Fig. 3. This ensures periodicity and continuity. Differentiability is not necessarily preserved but we do not notice behavior in the numerical simulations indicative of problems due to lack of differentiability. Upon studying Fig. 2, we see that most surface variations vary slowly with a mean amplitude (average absolute deviation from the mean height) of 4.6 nm. Relative to a length scale of $\lambda = 110$ nm, the surface amplitudes are small with a slow spatial modulation and we would expect the roughness to have a small effect. There are, however, very localized regions where the surface height changes rapidly and it is unclear if these regions could cause the non-exponential field profiles found in experiment.

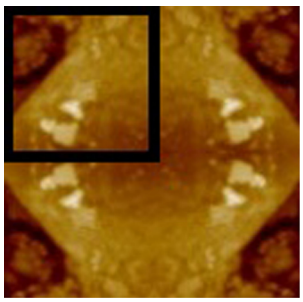

Fig. 3 Starting with an initial subset of the surface, we do reflections to produce an image that can be continuously extended periodically

Due to the discrete nature of the surface data in Section 3.3, it is not possible to refine the finite difference mesh arbitrarily. We choose to take small subsets of the surface where the mesh size can be as small as the AFM data allow.

2.2 Validation of Numerical Results

The previous framework was rigorously verified to be second-order convergent and to be consistent with a three-term asymptotic expansion (in roughness amplitude) for the magnetic field everywhere in space when provided with a sinusoidal surface roughness. In order to validate the modified numerical work, we can compare the results of the analytic approach with the discrete approach in the average field profiles they predict. The analytic approach was second-order accurate, and the discrete approach has been designed as such, by ensuring the discrete computation of the solution has an error, relative to the analytic code, that is smaller than second order for all surfaces of the form $z = \epsilon \cos(\omega_x x)\cos(\omega_y y)$. We verify that the maximum difference is indeed smaller than second order and that the discrete approach results converge to the analytic approach results. See Table 1 for an abridged convergence study.

2.3 Finding a Best Fit for the Penetration Depth and Dead Layer

In our numerical simulations, we assume the London penetration depth is precisely $\lambda_{\text{true}} = 110$ nm, but in the fitting, we seek to find values for λ and δ, the dead layer, so as to

Table 1 Verification that the discretely extended code converges to the sinusoidal code with $z = 0.05\cos(2\pi x)\cos(2\pi y)$

Discretization N	Max difference in profiles
3	2.2×10^{-2}
7	2.4×10^{-3}
15	3.0×10^{-4}

We compute the average field profiles in both versions of the code and calculate the maximum pointwise difference between the two predictions at different values of the mesh size which is $h = O(1/N)$. We validate that solutions of the two codes converge to each other at a rate of $O(h^{2.7})$ (through finding the slope of a log-log plot of the difference versus h), and given the sinusoidal code converged to the true solutions at rate $O(h^2)$, we conclude the same for the discretely extended code

minimize the sum of the residuals squared between the data set (z_i, B_i) and (z_i, f_i) where

$$f_i = \begin{cases} B & z_i < \delta \\ B\mathrm{e}^{-(z_i-\delta)/\lambda} & z_i \geq \delta, \end{cases}$$

$1 \leq i \leq N$. In this case, B_i represents the average field magnitude at depth z_i past the surface. Deviations in the best fit λ from λ_{true} illustrate how the true λ may be distorted due to surface roughness; positive values for the dead layer δ show that the roughness can produce a dead layer effect. We observe that most best-fitting dead layers are negative. For full clarity, we define the dead layer and penetration depth with the pseudocode given below:

- We begin with a set of numerically computed values for the average magnetic field B_i at depth z_i, all in dimensionless units so that a scaled field strength of $|\mathbf{B}_{\text{applied}}|$ have a value of 1 and a scaled distance of λ_{true} has a value of 1. We then choose a value of λ.
- For $1 \leq j \leq N-1$, we define

  $$\delta_j = \min\{z_{j+1}, \max\{z_j, \lambda \log(\frac{\sum_{k=j+1}^{N} B_k \mathrm{e}^{-z_k/\lambda}}{\sum_{k=j+1}^{N} \mathrm{e}^{-2z_k/\lambda}})\}\}$$

  to be the value of $\delta \in [z_j, z_{j+1}]$ that minimizes the sum of squares of the residuals. If the true minimizer lies to the left of the interval, the left endpoint is chosen, similarly with the right.
- For $1 \leq j \leq N-1$, we compute the sum of squares error with $\delta = \delta_j$ giving us $S_j = \sum_{k=1}^{j}(1-B_k)^2 + \sum_{k=j+1}^{N}(\mathrm{e}^{-z_k-\delta_j} - B_k)^2$.
- Compute $j^* = \arg\min_j S_j$ and define the dead layer for this λ to be $\delta_\lambda^* = \delta_{j^*}$.
- Iterate this procedure over different λ and determine the $(\lambda, \delta_\lambda^*)$ pairing that has the minimum sum of squares of all the cases.
- The dimensional quantities are then the above values multiplied by λ_{true}.

By giving the algorithm an input of a profile that is constant with value 1 up to a depth δ and which subsequently decays exponentially with dimensionless length scale λ, we find that the algorithm correctly calculates δ and λ.

3 Results

3.1 Large Scale Frequencies Present in the Surface

Through discrete Fourier analysis upon the surface as imaged in Fig. 2, we are able to determine the spatial frequency with the largest contribution to the surface geometry. For a surface $z_{j,k}$ measured at discrete indices (j, k) where $0 \leq j \leq N_x - 1$ and $0 \leq k \leq N_y - 1$, the two-dimensional discrete fourier transform is given by

$$c_{J,K} = \frac{1}{N_x N_y} \sum_{j=0}^{N_x-1} \sum_{k=0}^{N_y-1} \mathrm{e}^{-2\pi i(jJ/N_x + kK/N_y)} z_{i,j}$$

for $0 \leq J \leq N_x - 1, 0 \leq K \leq N_y - 1$. The original surface can be reconstructed from $c_{J,K}$ by

$$z_{i,j} = \sum_{J=0}^{N_x-1} \sum_{K=0}^{N_y-1} \mathrm{e}^{2\pi i(jJ/N_x + kK/N_y)} c_{J,K}.$$

Knowledge of the amplitudes of various (J, K)-frequencies gives us knowledge of how strong of a contribution different wavelengths have in creating the surface.

We found that beyond the $(0, 0)$-mode, i.e., the average value of the surface value, of 34.5 nm, the next most dominant mode was $(1, 2)$ with amplitude 0.9 nm. This implies that a sinusoidal surface with wavelength of 5 μm in the $x-$direction and 2.5μm in the $y-$direction had the strongest non-zero contribution to the field profile because the $(0, 0)$-mode has no effect on the field profile when plotted relative to the superconductor-vacuum interface.

From [14], it was found that for isotropic superconductors with purely sinusoidal surfaces, the effects of roughness generally increase with the spatial frequency and with the amplitude of the roughness. Even surface amplitudes on the order of 10 nm ($\gg$ 0.9 nm) and at frequencies yielding wavelengths on the order of 110 nm ($\ll$ 2.5μm, 5 μm) scarcely yielded dead layer phenomena. Based solely upon this analysis, it seems unlikely that large scale surface details of the superconductor account for the dead layer. However, it is possible that the local surface features, the peaks and valleys that occur on small length scales, do somehow bring about the experimental results. The remainder of this paper explores the local, non-sinusoidal effects of the surface roughness.

3.2 Overview of Small Scale Surface Feature Analysis

We compute the field profiles for different localized surface geometries and observe the field orientation. In all cases, we assume the underlying London penetration depth is $\lambda_{\text{true}} = 110$ nm. Through the simulations, we consider the average field magnitude as a function of depth (denoted by s). Note that s is not the $z-$position, but the $z-$displacement with respect to the superconductor surface with $s < 0$ for vacuum and $s > 0$ for superconductor. Precisely, $s = z - f(x, y)$. The profiles are averaged over x and y. Through the average field magnitude profiles, we estimate the best fitting dead layer δ and London penetration depth λ as described above in Section 2.3. By a dead layer, we refer to a depth δ so that if $s < \delta$ then the average field magnitude is constant and equal to its applied value and if $s > \delta$ then the average field

magnitude decays exponentially from its applied value with length scale λ. This analysis gives insight into how much the measured value of λ differs from the true value when surface roughness is considered. We remark that in the actual experiments, the field is not measured in the vacuum $s < 0$, however, the numerical simulations do give this flexibility. As has been found in [14], the magnetic field magnitude in general decreases before reaching the superconductor surface and as a result many best-fitting dead layers appear to be slightly negative. Other experiments in the future could entail coating the superconductor with silver, which would allow for a measurement of the field in the $s < 0$ region.

3.3 YBCO Field Profiles

The full surface is depicted in Fig. 4, but we only analyze small subsets. We take eight subsets of the surface shown in Fig. 5. In some cases, we consider different orientations of the subset as explained in the figure. Through analyzing these subsets, we can assess how the actual surface of YBCO could affect the field profile and experimentally measured dead layers and penetration depths.

The dead layers and penetration depths predicted for subsets 1-8 are given in Table 2. As we can observe, the dead layers are much smaller than the 10 nm measured in experiments [7], and are in fact mostly negative. This is a result of the fact that the magnetic field in general decays slightly in magnitude before reaching the interface and a negative dead layer captures this phenomena better. We also observe that in general, the best fitting penetration depth is smaller than λ_{true} by roughly 5 %. It is interesting to remark that the roughness orientation is important: subsets 3 and 4 are transposes of each other, as are subsets 6 and 7. In both cases, while the λ values are similar, the values of δ change sign. Furthermore, subsets 3 and 6 are reflections of each other (with respect to depth), just as 4 and 7 are, and both fit parameters of λ and δ are quite similar in value.

We provide plots of the average field magnitude and standard deviation in field magnitude of the two cases tabulated

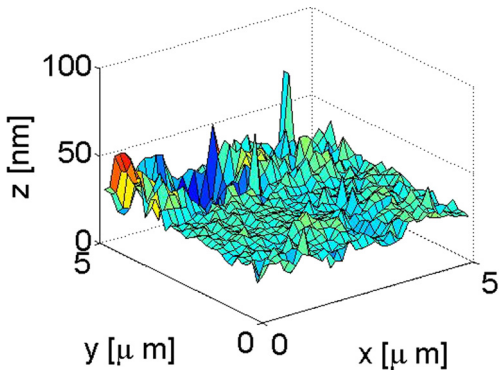

Fig. 4 This is what the full $YBa_2Cu_3O_x$ surface looks like after it has been converted to a surface. Only every sixteenth point was plotted

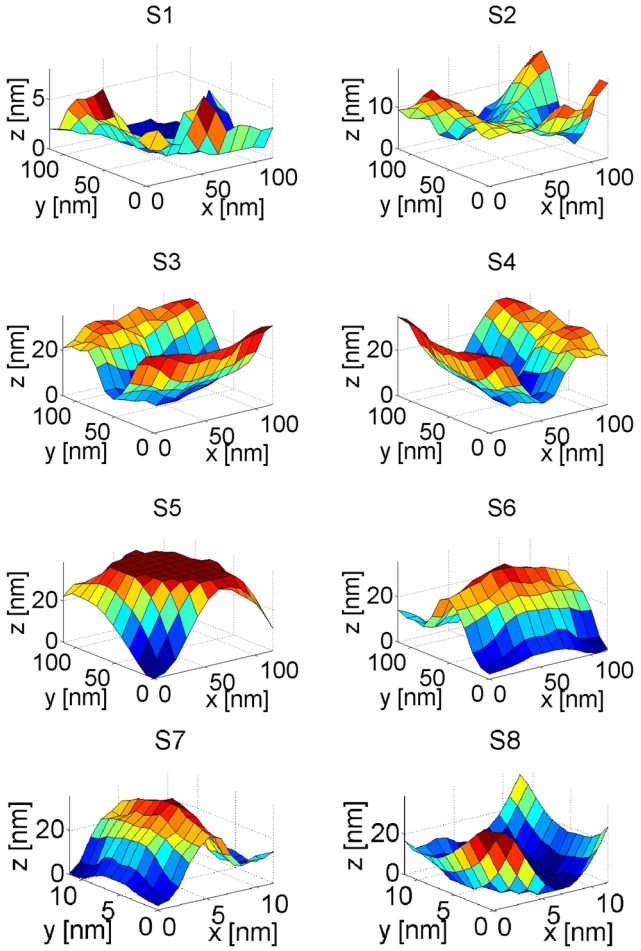

Fig. 5 The subsets of the original surface considered. A higher resolution is not possible here as we are making use of pixel-by-pixel information at this point. The full surface can be seen in Fig. 4. Subsets S1 and S2 are from regions that are reasonably flat. Subset S3 appears to have a reasonably large bump with an axis of symmetry in the x-direction and subset S4 is its transpose with respect to x and y so that its axis is in the y-direction. Subset S5 was taken near a local maximum in the surface amplitude, appearing reasonably symmetric in x and y. By inverting subsets S3–S5 with respect to z, subsets S6-S8 are generated, respectively. The surfaces are positioned such that their minimum value is $z = 0$. An upward and downward surface direction point into and out of the superconductor, respectively

Table 2 Best fit parameters for subsets of $YBa_2Cu_3O_x$ sample surface

Subset	London Depth [λ_{true}]	Dead Layer [λ_{true}]
S1	1.000	0.000
S2	0.987	0.001
S3	0.956	0.015
S4	0.951	-0.016
S5	0.960	-0.012
S6	0.956	0.016
S7	0.951	-0.016
S8	0.960	-0.009

All parameters are scaled relative to λ_{true}

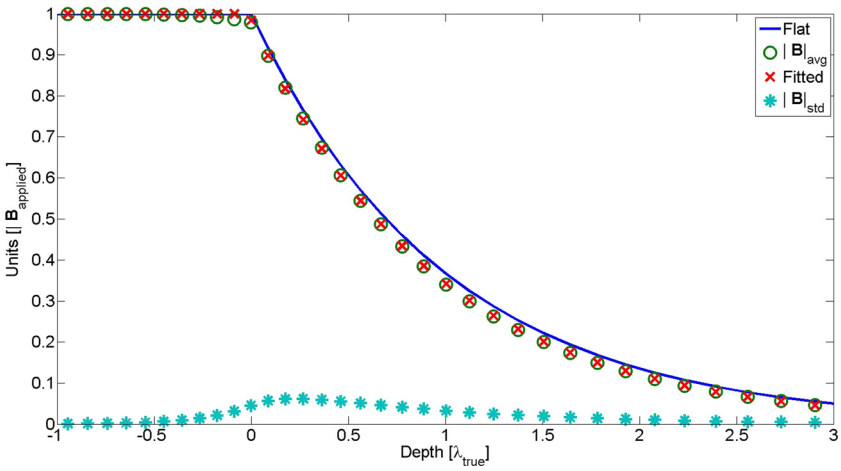

Fig. 6 For subset S4, we plot the profiles of the average field magnitude ($|\mathbf{B}|_{\text{avg}}$), the standard deviation in the average field ($|\mathbf{B}|_{\text{std}}$), the average field profile for a flat superconductor with $\lambda = \lambda_{\text{true}}$ ("Flat"), and the fitted field profile with best fitting λ and δ ("Fitted")

in Table 2 with the largest positive and largest negative dead layers: subset 4 and subset 6. As we can observe in Figs. 6 and 7, all the profiles begin with the applied field value and then decay slightly in the vacuum region (where the depth $s < 0$). Within the superconductor, the field magnitude is initially very close to, but then decays slightly faster than, the profile of a flat superconductor with $\lambda = \lambda_{\text{true}}$. In [14], the higher field value was noted near the interface, but in the case of the sinusoidally modulated surfaces, even deep within the superconductor, the rough field profile was larger. We speculate that this may be a result of the highly symmetric nature of a purely sinusoidal surface, the effect of which is lost when the surface has many Fourier modes: although the first-order correction in an asymptotic expansion is linear in the Fourier components, the higher order corrections are nonlinear in the respective Fourier modes due to cross-terms as seen in [14]. We also observe the highest variance in the field magnitude just past the interface. This stands to reason: near where the field is applied, there should be no variation and deep in the superconductor where the field strength decays to zero, there should also be no variation. As the decay is most pronounced within the superconductor, this is where we would expect to see large fluctuations in field strength at different x or y values at a fixed depth. Thus, the peak variance should be a little inside of the superconductor.

3.4 Field Orientation

One of the most interesting results from [14] was that due to roughness, the field orientation is perturbed. The field does not remain parallel to its applied direction throughout the superconductor. We remark that this is a key assumption in the interpretation of experimental data: the magnetic field is assumed always to point in the same direction with fluctuations in magnitude at a given depth following Gaussian distributions [16].

Based on the numerical simulations, we plot the probability density functions for various parameters of interest for the magnetic field at various depths for subset 6 (Fig. 8).

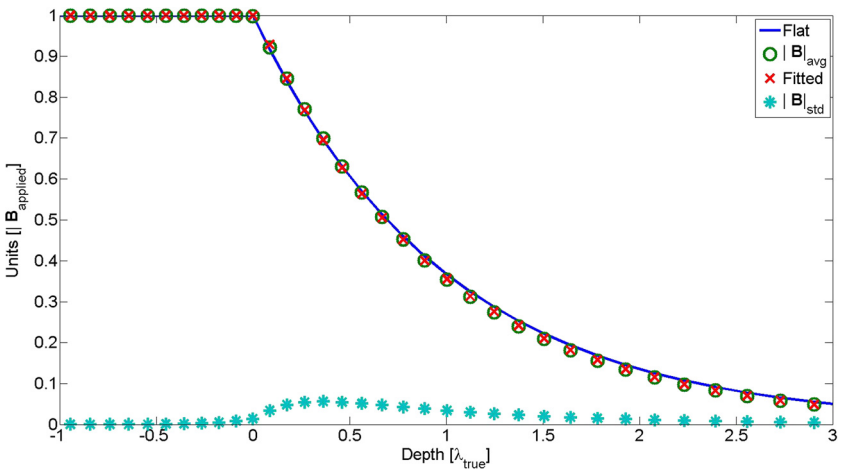

Fig. 7 For subset S6, we plot the profiles of the average field magnitude ($|\mathbf{B}|_{\text{avg}}$), the standard deviation in the average field ($|\mathbf{B}|_{\text{std}}$), the average field profile for a flat superconductor with $\lambda = \lambda_{\text{true}}$ ("Flat"), and the fitted field profile with best fitting λ and δ ("Fitted")

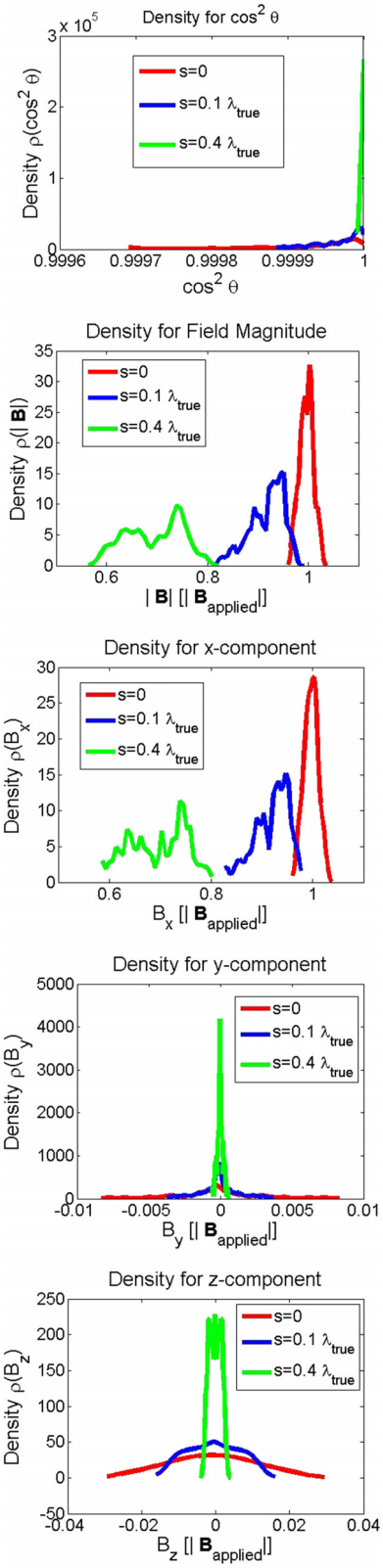

Fig. 8 The probability density function (pdf) of $\cos^2\theta$ describes the pdf of the value of $\cos^2\theta$ where θ is the angle between the local magnetic field and the applied field direction. The pdfs for the field magnitude, and individual x-, y-, and z-components are also displayed. We considered three depths: $s = 0\lambda_{\text{true}}$, $s = 0.1\lambda_{\text{true}}$, and $s = 0.4\lambda_{\text{true}}$

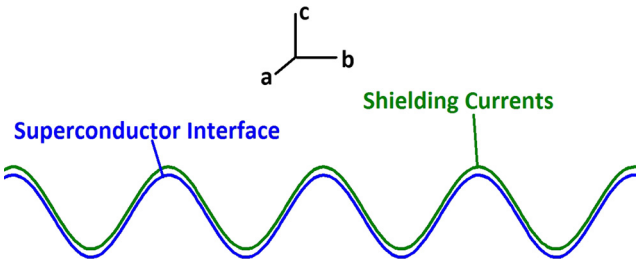

Fig. 9 Shielding supercurrents should flow parallel to the superconducting interface

These probability density plots are generated with a Matlab routine for kernel density estimation kde; this technique allows for an estimation of a probability density function (pdf) without making any assumptions about the underlying distribution.

The pdfs are both interesting and intuitive. If θ denotes the angle between the applied field direction and the magnetic field direction at a given depth, then from the pdf of $\cos^2\theta$, we observe that the angle is heavily peaked near $\theta = 0$ and that the spread decreases with depth. Our choice of $\cos^2\theta$ as a parameter of interest instead of simply the angle θ is due to the $\cos^2\theta$ reflecting the signal strength due to the muons in experiments precessing about an axis orthogonal to their polarization direction; the bigger this value, the more that a signal in the experiments can be attributed to the size of the magnetic field magnitude in the direction of the applied field. We affirm that the assumption that the magnetic field remains parallel to the applied field is quite accurate. Also, given that experiments cannot measure local magnetic properties right at the surface of a superconductor but rather at some finite depth inside, the assumption of the field remaining parallel to its applied direction appears to be even more valid in experimental interpretation.

The plots of the pdfs for the field magnitude and components are not Gaussian. With increasing depth, the average field values decrease in magnitude, consistent with a decay in field magnitude. It is interesting that the spreads in magnetic field $y-$ and $z-$component values decrease but the spread for the $x-$component value increases with depth.

4 Conclusions

Based on the experimental data of $YBa_2Cu_3O_x$ surface roughness, we have studied and made predictions about the effects roughness induces upon an isotropic type II superconductor.

The surface roughness causes an effect that is often not considered experimentally that of a changing field orientation. Our results suggest, however, that despite the changing

field orientation in this model, such effects may very well be negligible.

Through experimental measurements, the dead layer for $YBa_2Cu_3O_x$ appears to be on the order of 10 nm [7], which is much bigger than the dead layers that could be attributed to the surface roughness given by the AFM measurements of YBCO within the isotropic London model. On average, we anticipate the figures provided in Table 2 to be accurate predictors of how actual surface roughness could affect the fit values of λ and δ within an isotropic London model. We find that while the dead layers are effectively negligible for the AFM field profile predictions, the best fit value of λ is slightly smaller than its true value. We also note, however, that experimental fits have a non-negligible dead layer, which we do not obtain in our fitting.

We conclude that in order to explain the dead layer phenomena in $YBa_2Cu_3O_x$, it may be necessary to use the fully anisotropic model. The main point is that in order to flow parallel to the interface, supercurrents would need to have a non-negligible component in the c-axis direction. If there is a strong anisotropy such that currents are heavily impeded in the c-direction, we expect the shielding would be much less effective and the field should not decay until after the roughness, see Fig. 9. Given that the surface roughness is on the order of 4.6 nm (average absolute deviation from mean surface height), it seems possible the roughness in combination with the anisotropy causes the dead layer. Such an analysis could in principle be done by further extending the numerical framework developed in this study.

It may also seem appropriate to consider the effects of the coherence length ξ in $YBa_2Cu_3O_x$ on the field profile with the Ginzburg-Landau equations. This has a dramatic effect on the field profiles in type I superconductors where λ and ξ are comparable [17]. That is not the case in YBCO where the coherence length much smaller than lambda even smaller than the deadlayer. Although we have not considered such equations here, given the coherence length for $YBa_2Cu_3O_x$ is approximately 1.3 or 1.6 nm [4, 18], it would be surprising for such a small length scale to give rise to an effect as large as the dead layers measured in experiments. Another potential explanation for the dead layer could be the suppression of the order parameter near the interface [19], due to subtle changes in chemical composition near the surface.

We finally comment that this isotropic analysis could be appropriate in understanding measurements of more isotropic type II superconductors such as Rb_3C_{60}. The superconductor Rb_3C_{60} has a cubic structure such that isotropy can be assumed with $\lambda \approx 247$ nm and a small coherence length $\xi \approx 2$ nm [20–22]. The isotropic London model should apply very well in this situation, and we would not expect a dead layer if μSR were used to measure the field profile.

Acknowledgments The authors would like to thank Pinder Dosanjh for help with the AFM imaging and the reviewer for helpful feedback in revising this manuscript.

References

1. Kittel, C.: Introduction to solid state physics. Wiley (1976)
2. Kogan, V.G.: Phys. Rev. B **24**, 3 (1980)
3. Du, Q., Gunzburger, M.D., Janet, S.: SIAM **34**, 1 (1992)
4. Akir, B., Aydiner, A., Karaoglu, K., Duman, S., Yanmaz, E.: JOSC **27**, 5 (2014)
5. Basov, D.N., Liang, R., Bonn, D.A., Hardy, W.N., Dabrowski, B., Quijada, M., Tanner, D.B., Rice, J.P., Ginsberg, D.M., Timusk, T.: Phys. Rev. Lett. **74**, 598 (1995)
6. Pereg-Barnea, T., Turner, P.J., Harris, R., Mullins, G.K., Bobowski, J.S., Raudsepp, M., Liang, R., Bonn, D.A., Hardy, W.N.: Phys. Rev. B **69**, 18 (2004)
7. Kiefl, R.F., Hossain, M.D., Wojek, B.M., Dunsiger, S.R., Morris, G.D., Prokscha, T., Salman, Z., Baglo, J., Bonn, D.A., Liang, R., Hardy, W.N.: Phys. Rev. B **81**, 18 (2010)
8. Ofer, O., Baglo, J.C., Hossain, M.D., Kiefl, R.F., Hardy, W.N., Thaler, A., Kim, H., Tanatar, M.A., Canfield, P.C., Prozorov, R., Luke, G.M.: Phys. Rev. B **85**, 6 (2012)
9. Sonier, J.E., Brewer, J.H., Kiefl, R.F.: Rev. Mod. Phys. **72**, 3 (2000)
10. Liang, R., Bonn, D.A., Hardy, W.N.: Physica C **304**, 105 (1998)
11. Doiron-Leyraud, N., Proust, C., LeBoeuf, D., Levallois, J., Bonnemaison, J., Liang, R., Bonn, D.A., Hardy, W.N., Taillefer, L.: Nature **447**, 565 (2007)
12. Bobowski, J.S., Baglo, J.C., Day, J., Dosanjh, P., Ofer, R., Ramshaw, B.J., Liang, R.X., Bonn, D.A., Hardy, W.N., Luo, H.Q.: Phys. Rev. B **82**, 9 (2010)
13. Stilp, E., Suter, A., Prokscha, T., Salman, Z., Morenzoni, E., Keller, H., Katzer, C., Schmidl, F., Dbeli, M.: Phys. Rev. B **89**, 2 (2014)
14. Lindstrom, M., Wetton, B., Kiefl, R.: J. Eng. Math. **85**, 1 (2014)
15. Dosanjh, P. (private communication)
16. Kiefl, R.F., Brewer, J.H., Carolan, J., Dosanjh, P., Hardy, W.N., Kadono, R., Kempton, J.R., Krahn, R., Schleger, P., Yang, B.X., Zhou, H.: Phys. Rev. B **63**, 19 (1989)
17. Suter, A., Morenzoni, E., Garifianov, N., Khasanov, R., Kirk, E., Luetkens, H., Prokscha, T., Horisberger, M.: Phys. Rev. B **72**, 2 (2005)
18. Jiang, H., Yuan, T., How, H., Widom, A., Vittoria, C.: J. Appl. Phys. **73**, 10 (1993)
19. Piovarci, S., Antala, V., Kanuchova, M., Radusovska, M.I., Diko, P.: (unpublished) (2014)
20. Alloul, H., Lyle, S.: Introduction to the Physics of Electrons in Solids (Springer Science & Business Media (2010)
21. Fleming, R.M., Ramirez, A.P., Rosseinsky, M.J., Murphy, D.W., Haddon, R.C., Zahurak, S.M., Makhija, A.V.: Nature **352**, 787 (1991)
22. Poole, C., Horacio, A., Creswick, R.J.: Handbook of superconductivity (Academic Press, 1999)